

1717. Dynamic coupled vibration analysis of a large wind turbine gearbox transmission system

Zhaohui Ren¹, Shihua Zhou², Bangchun Wen³

School of Mechanical Engineering and Automation, Northeastern University, Shenyang, 110819, China

²Corresponding author

E-mail: ¹zhhren.neu@gmail.com, ²zhou_shihua@126.com, ³bcwen1930@sina.com.cn

(Received 11 April 2015; received in revised form 2 June 2015; accepted 18 June 2015)

Abstract. A lumped-parameter coupled nonlinear dynamic model for one large multi-stage wind turbine gearbox transmission system is established comprehensively including wind varying load, mesh stiffness, dynamic transmission error, gravity, and bearing nonlinear characteristics to obtain the gearbox dynamic response. The vibration differential equations of the drive-train are deduced through the Lagrange's equation. On the basis of that, the dynamics of wind turbine gearbox is investigated by a Runge-Kutta numerical method that includes simultaneous internal and external excitations. The results show that the dynamic response of the partial component is mainly superposed by high-frequency component caused by the internal excitation and low-frequency component caused by the external excitation. In medium-speed stage and high-speed stage, the vibration amplitude has obvious fluctuation, and the multiple frequency and random frequency components become increasingly obvious with increasing rotational speed and eccentricity at gear and bearing positions. Axial vibrations of the system also have some fluctuation. The bearing has self-variable stiffness frequency, which should be avoided in engineering design stage. The study results provide a theoretical foundation for dynamical characteristics evaluation and dynamic optimization of a large wind turbine gearbox transmission system.

Keywords: wind turbine gearbox, dynamical model, coupled vibration, dynamic response.

1. Introduction

The gearbox transmission plays an important role in wind power industry. A failure of the transmission may cause breakdown of the whole machinery and major economic loss. Wind turbine is being increasingly deployed in remote onshore and offshore areas due to the richer wind resource and the advantages of mitigating the land use and visual impact issues. In addition, it is complex aerodynamic, mechanical and electrical machines incorporating sophisticated control systems. Therefore, dynamic coupled vibration analysis of a large wind turbine gearbox is a key research topic in the operation and maintenance of the gearbox system, which is consist of housing, shaft, gear, support bearing and so on. The study of the vibration characteristics of individual component has been established an important part of the design. However the vibration characteristics of an individual component can change considerably when these components are assembled together to form one system, due to the coupled vibration effects among these constituent components. The gearbox is the key equipment of the synthetically mechanized wind turbine equipment, the dynamic performance impacts on the reliability and safety of the whole wind turbine. The accuracy dynamic response analysis of the wind turbine gearbox transmission is also gradually increased due to the development of power for the wind turbine train system towards the MW. Hence, the research of the coupled nonlinear dynamics an important theoretical significance and engineering application value for the large wind turbine gearbox provides. A number of models were proposed in past to describe the dynamic behavior of the wind turbine gearbox transmission system, and also achieved some remarkable achievements [1-19]. Riziotis V. A. [4] and Thomsen K. [5] established the coupled nonlinear dynamic model of a multi-stage gear-rotor-bearing transmission system by considering the internal and external excitation, and the dynamic response of the typical system is calculated and analyzed with modal superposition method. Peeters J. [6] presented three types of multi-body models for the investigation of a drive train in a wind turbine, and a comparison of the different modeling

techniques is discussed for a wind turbine's drive train with a helical parallel high speed stage, two planetary stages and a flexible rotor. Yang [7] developed an effective method for processing raw SCADA data from wind turbine, proposed an alternative condition monitoring technique based on investigating the correlations among relevant SCADA data, and realized the quantitative assessment of the health condition of a turbine under varying operational conditions. Pérez J. [8] categorized the main designs, focusing on their reliability by bringing together and comparing data from a selection of major studies due to wind turbine manufacturers are continuing to develop a range of configurations with different combinations of pitch control, rotor speeds, gearboxes, generators and converters. Tavner P. J. [9] and Zhou [10] discussed the practical methods of predicting large-wind-turbine reliability using grouped survey data from wind stats and show the turbine design, turbine configuration, time, weather and possibly maintenance can affect the extracted results. Zhu [11] and Bartelmus [12] analyzed the transmission system of gearbox used in a large-scaled wind-driven generator with application of the theory of engagement, gear system dynamics and nonlinear dynamics, and the nonlinear coupling dynamic system with multi-speed gear-driven, which includes the gears, shafts and housing, was established including time-varying stiffness, running clearance and manufacturing errors. Besides, the dynamic behaviors of the coupled system were analyzed when the internal excitation to the system was considered. Qin [13, 14] developed a mathematical model of a horizontal wind turbine drive-train by applying the flexible multi-body dynamics theory based on the Lagrange's equation. The natural frequencies and modes were calculated, and the effects of bearing stiffness on those modes were examined. The rotational vibrations of the sun gears as well as the tooth contact forces between the sun and planet and the ring and planet were analyzed in detail. Xu [15] established the dynamic model of overall gearbox train system by lumped parameter method including the time-varying, comprehensive mesh stiffness, meshing error, and coupled vibration. But this article did not give the corresponding numerical simulation. Helsen [16-17] and John [18] focused on the gearbox model behavior assessment by means of three more complex modeling techniques of varying complexity. Both simulation and experimental results were discussed. Typical mode categories for traditional wind turbine gearboxes were defined. Moreover the challenge of the definition of an accurate approach to condense finite element models for representing the flexible components in the flexible multi-body models was overcome. Shi [19] established a mathematical model for a horizontal axial wind turbine drive-train using the torsional multi-body dynamic model. The differential equation was solved numerically by direct numerical integration, and dynamic analysis was carried out to investigate the transient response of the drive-train system. It can be seen that the references made summaries, comparison, and researches on the dynamical characteristics of the gearbox transmission system in the past, the coupled dynamic model of the gearbox system for wind turbine which considers the external load excitation, meshing stiffness, input and output torques, meshing error, nonlinear characteristics of the support bearing and gravity is rare. In order to analyze the dynamic characteristics of the gearbox transmission system more accurately, it is necessary to establish precise dynamic model of the gearbox transmission system. A requirement for reliable gearbox design calculations is sufficient insight in the dynamics of the entire wind turbine drive train.

Accurate analytical modeling, including mesh relationships and detailed characterization of the nonlinear dynamics of wind turbine gearbox, is needed to estimate gearbox vibration and predict dynamic forces in industrial applications. Little work has been done to characterize for the nonlinear effects of the support bearing and gravity on gearbox dynamics. The lack of experiment studies to understand the complex dynamics of gearbox. In this paper, characterize the complex, nonlinear dynamics of gearbox transmission system by lumped-parameter method propose an analytical model, which is systematically studied the vibration characteristics of wind turbine gearbox transmission system.

2. Dynamic model and equations of gearbox

The theoretical system structure and the physical model are shown in the Fig. 1(a) and (b) respectively. The MW wind turbine gearbox transmission system that will be studied in this paper, as shown in Fig. 2, is a structural diagram that is a multi-mesh gear train. The drive-train in this study consisted of a low-speed planetary gear stage (three identical planets with spur teeth, sun and fixed ring gears) and two high-speed helical gear stages. This typical arrangement has been commonly used in the wind turbine industry.

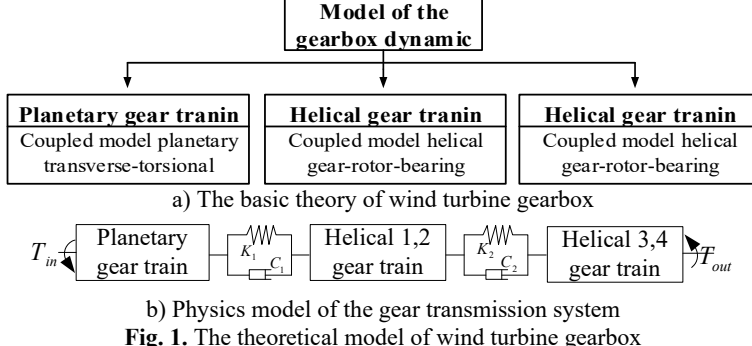


Fig. 1. The theoretical model of wind turbine gearbox

In Fig. 2, T_{in} is the input torque, T_{out} represents the output torque, P_i indicates the planet gear, c is the carrier, r indicates the ring gear, s is the sun gear, 1 and 2 represent the driving and driven gears of intermediate-speed stage, 3 and 4 are the driving and driven gears of high-speed stage.

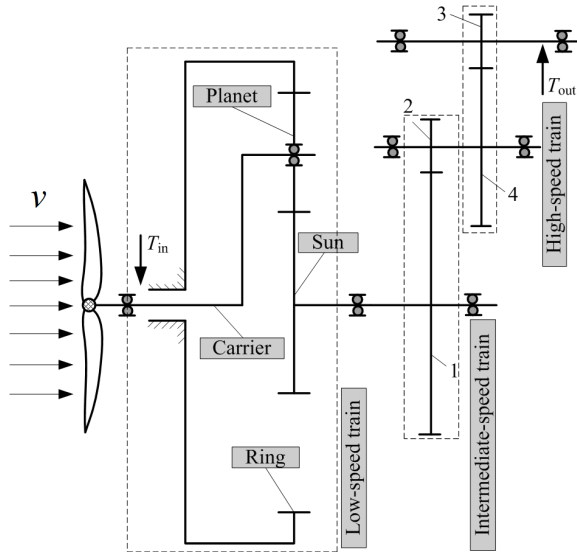


Fig. 2. Structure diagram of wind turbine gearbox transmission

2.1. Lumped-parameter analytical model of helical gear

Considering the influence of input/output and support bearing, et al., the static model of helical gear-shaft-bearing system is shown in Fig. 3. The dynamic model of the transmission system, as shown in Fig. 4, is established. m_1 and m_2 are the equivalent mass of helical gears respectively. J_1 and J_2 represent moment of inertia; m_{bi} ($i = 1-4$) is equivalent mass at bearing position. J_d and J_l indicate moment of inertia in input/output terminal. ρ_1 and ρ_2 represent the eccentricity. F_{xi} ,

F_{yi} and F_{zi} ($i = 1-4$) are nonlinear bearing forces in x , y and z directions.

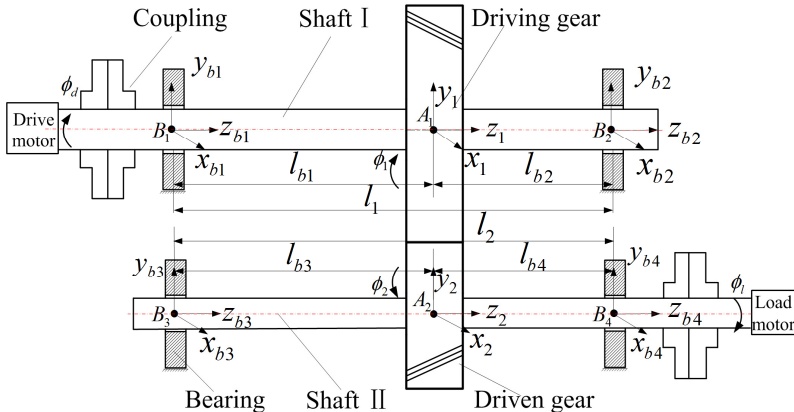


Fig. 3. Static model of helical gear-rotor-bearing system

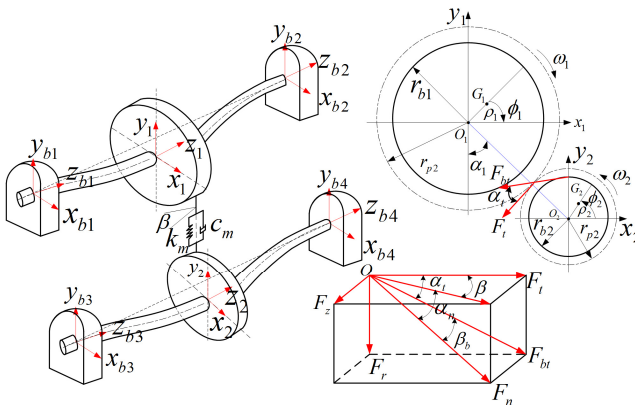


Fig. 4. Dynamic mode of helical gear-rotor-bearing system

In Fig. 3, the fixed coordinate system $A_i-x_iy_iz_i$ ($i = 1, 2$) is set up at A_i , which is the ideal center of the helical gears. B_i ($i = 1-4$) represents the ideal center of bearing. $O_1(x_1, y_1, z_1)$ and $O_2(x_2, y_2, z_2)$ are the geometric rotational centers of the driving and driven gears; $G_1(x_{g1}, y_{g1}, z_{g1})$ and $G_2(x_{g2}, y_{g2}, z_{g2})$ represent centroid respectively. To deduce kinetic equations of the helical gear-shaft-bearing system, the stress of the cylindrical gear with helical teeth should be analyzed primarily. Therefore, the dynamic model of gear meshing is shown in Fig. 4. Φ_1 and θ_1 ($j = 1, 2, d, l$) are the rotation angle and angular vibration displacement of driving gear, driven gear, input terminal and output terminal. r_{b1} and r_{b2} are the base radius of driving and driven gears respectively; F_t , F_r and F_a represent the tangential force; radial force and axial force. α_t and α_n are the pressure angles of the pitch circle in the end face and normal direction. β and β_t are helix angles of pitch circle and base circle. α_1 indicates the angle between center line and vertical direction.

According to the previous geometrical relationship, the angle displacements of the input/output, driving and driven gears can be expressed by the following equations:

$$\phi_d = \omega_1 t + \theta_d, \quad \phi_l = \omega_2 t + \theta_l, \quad \phi_1 = \omega_1 t + \theta_1, \quad \phi_2 = \omega_2 t + \theta_2. \quad (1)$$

The relationships between $G_1(x_{g1}, y_{g1}, z_{g1})$, $G_2(x_{g2}, y_{g2}, z_{g2})$ and the $O_1(x_1, y_1, z_1)$, $O_2(x_2, y_2, z_2)$ are expressed as follows:

$$\begin{aligned}x_{g1} &= x_1 + \rho_1 \cos(-\phi_1), \quad x_{g2} = x_2 + \rho_2 \cos\phi_2, \\y_{g1} &= y_1 + \rho_1 \sin\phi_1, \quad y_{g2} = y_2 + \rho_2 \sin(-\phi_2), \\z_{g1} &= z_1, \quad z_{g2} = z_2.\end{aligned}\quad (2)$$

In order to ensure the contact of teeth surface on meshing performance, it is assumed that the relative deformation of gear pair is completely changed into elastic deformation on teeth surface along with the meshing direction. The meshing gear pair is connected through the spring and damper [20]. Therefore, the comprehensive deformation of two helical gears in the meshing direction is expressed as:

$$\delta = (r_{b1}\theta_1 - r_{b2}\theta_2) + [(x_1 + \rho_1 \cos\phi_1) - (x_2 + \rho_2 \cos\phi_2)] \cos(\alpha_1 - \alpha_t) + [(y_1 - \rho_1 \sin\phi_1) - (y_2 + \rho_2 \sin\phi_2)] \cdot \sin(\alpha_1 - \alpha_t) + (z_1 - z_2) \tan\beta - e(t). \quad (3)$$

Based on the viscoelasticity theory, the meshing force of gear can be described as:

$$F = c_m \dot{\delta} + k_m \delta, \quad (4)$$

where k_m and c_m represent the average meshing stiffness and damping; r_{b1} and r_{b2} indicate the base radius of helical gears; $e(t)$ is the meshing error.

It is assumed that the dynamic meshing force which is from the driving gear to the driven gear is positive. So the meshing forces in x , y and z directions can be described respectively as:

$$F_x = F \cos(\alpha_1 - \alpha_t), \quad F_y = F \sin(\alpha_1 - \alpha_t), \quad F_z = F \tan\beta. \quad (5)$$

2.2. Lumped-parameter analytical model of planetary gear

The planet carrier is regarded as the input terminal, and the sun gear is the output terminal. The gear mesh is modeled as linear spring acting along the pressure line direction. The other supports/bearings are modeled as nonlinear springs. The friction forces due to gear teeth contact and other dissipative effects are captured using modal damping. Therefore the translational-rotational model of the planetary gear system is shown in Fig. 5.

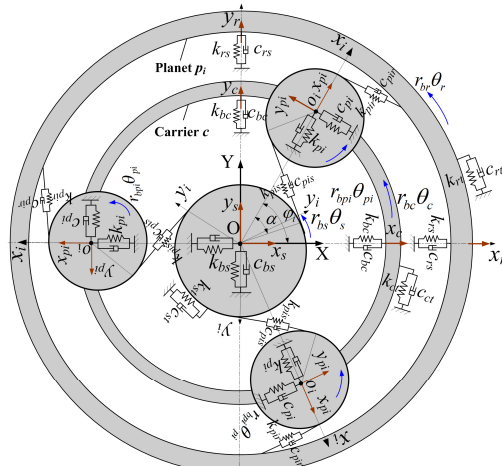


Fig. 5. The dynamic model of planetary transmission system

In Fig. 5, the OXY is the fixed-coordinate system. Oxy represents the motional-coordinate system of the planet carrier. The Ox_i points to the theory center of the planet gear, and the ideal angular velocity of the carrier is ω_c . s, r, c, p_i are the subscripts of the sun, ring, carrier and planet

respectively, and the subscripts from $1-i$ ($i = 1, 2, 3$) designate the planets. x_j, y_j ($j = s, r, c$) represent the lateral displacements (the projections in the fixed coordinate system OXY). x_{pi}, y_{pi} ($i = 1, 2, 3$) indicate the vibration displacements projections of the i th planet gear in $o_{pi}x_{pi}y_{pi}$ coordinate system. r_{bj} ($j = s, r, c, p_i$) is the base radius of gears or radius of the carries. θ_j ($j = s, r, c, p_i$) represents the rotational displacement of the sun, ring, carrier and planet respectively. Besides, it is assumed that the counterclockwise is the positive direction. φ_i is the circumferential position of the i th planet around the sun gear and $\varphi_i = 2\pi(i-1)/n$, α is the sun-planet and ring-planet operating pressure angles. k_{sj}, c_{sj} ($j = s, t, b$) are the bending, torsional of sun gear and the bearing stiffness and damping in x -direction and y -direction respectively, k_{rj}, c_{rj} ($j = s, t$) represent the bending of ring and the bearing stiffness and damping in x -direction and y -direction, k_{cj}, c_{cj} ($j = s, t, b$) indicate the bending, torsional of the carrier and the bearing stiffness and damping in x -direction and y -direction respectively, k_{bpi}, c_{bpi} are the i th bearing stiffness and damping of planet gear in lateral-direction, $k_{pis}, c_{pis}, k_{pir}, c_{pir}$ are the mesh stiffness and damping of sun-planet and ring-planet in the pressure line direction.

2.2.1. The elastic deformation of sun-planet in the pressure line direction

In the paper x_s, y_s are the linear displacements of the sun gear in x -direction and y -direction, and the $\theta_s r_{bs}$ is the circumferential angular displacement. $x_s \sin \varphi_{si}, -y_s \cos \varphi_{si}$ and $-\theta_s r_{bs}$ are the projections of sun-planet along the pressure line direction. x_{pi}, y_{pi} are the linear displacement of the planet gear in x -direction and y -direction, and the $\theta_{pi} r_{bpi}$ is the circumferential angular displacement. $x_{pi} \sin \alpha, -y_{pi} \cos \alpha$ and $-\theta_{pi} r_{bpi}$ are the projections of sun-planet along the pressure line direction. So the compressive deflections in the sun-planet mesh spring can be expressed as follows:

$$\delta_{pis} = x_s \sin \varphi_{si} - y_s \cos \varphi_{si} - r_{bs} \theta_s + x_{pi} \sin \alpha + y_{pi} \cos \alpha - r_{bpi} \theta_{pi}, \quad (6)$$

$$\varphi_{si} = \varphi_i - \alpha.$$

2.2.2. The elastic deformation of ring-planet in the pressure line direction

x_r, y_r are the linear displacement of the ring in x -direction and y -direction, and the $\theta_r r_{br}$ is the circumferential angular displacement. $x_r \sin \varphi_{ri}, -y_r \cos \varphi_{ri}$ and $-\theta_r r_{br}$ are the projections of ring-planet along the pressure line direction. x_{pi}, y_{pi} are the linear displacement of the planet gear in x -direction and y -direction, and the $\theta_{pi} r_{bpi}$ is the circumferential angular displacement. $-x_{pi} \sin \alpha, y_{pi} \cos \alpha$ and $\theta_{pi} r_{bpi}$ are the projections of ring-planet along the pressure line direction. So the compressive deflections in the ring-planet mesh spring can be expressed as follows:

$$\delta_{pir} = x_r \sin \varphi_{ri} - y_r \cos \varphi_{ri} - r_{br} \theta_r - x_{pi} \sin \alpha + y_{pi} \cos \alpha + r_{bpi} \theta_{pi}, \quad (7)$$

$$\varphi_{ri} = \varphi_i + \alpha.$$

2.2.3. The relative elastic deformation between planet gear and carrier

δ_{pix} and δ_{piy} are the relative displacement between planet gear and carrier in the ox_iy_i coordinate system, the elastic deformations are:

$$\delta_{pix} = x_{pi} - x_c \cos \varphi_i - y_c \sin \varphi_i, \quad \delta_{piy} = y_{pi} + x_c \sin \varphi_i - y_c \cos \varphi_i - r_{bc} \theta_c. \quad (8)$$

2.3. Vibration differential equations of the wind turbine gearbox transmission system

Based on the dynamic models of the helical gear and the planetary gear transmission, a

generalized displacement vector of the whole gearbox transmission system can be defined with respect to the global co-ordinate system by:

$$A = r_i + r_o + \gamma_0 - d_b, \quad (9)$$

where θ_i ($i = c, r, p_i, s, 1, 2, 3, 4$) represent the angular vibration displacement respectively, x_i, y_i, z_i ($i = c, r, p_i, s, 1, 2, 3, 4$) are the linear vibration displacements in x, y, z directions.

According to the dynamic analysis of the wind turbine gearbox, taking into the mesh stiffness, input/output torque, the kinetic energy T , the potential energy U and the dissipation function R , are established of the gearbox system. Utilizing the Lagrange equation, the differential equations of the train system can be expressed as follows:

The vibration differential equation of the carrier:

$$\begin{aligned} m_c \ddot{x}_c + 2c_{cs}(\dot{x}_c - \dot{x}_{bc}) - \sum_{i=1}^3 c_{pi}(\dot{\delta}_{pix} \cos \varphi_i - \dot{\delta}_{pix} \cos \varphi_i) + 2k_{cs}(x_c - x_{bc}) \\ - \sum_{i=1}^3 k_{pi}(\delta_{pix} \cos \varphi_i - \delta_{pix} \cos \varphi_i) = F_{bcx}, \\ m_c \ddot{y}_c + 2c_{cs}(\dot{y}_c - \dot{y}_{bc}) - \sum_{i=1}^3 c_{pi}(\dot{\delta}_{pix} \sin \varphi_i + \dot{\delta}_{pix} \cos \varphi_i) + 2k_{cs}(y_c - y_{bc}) \\ - \sum_{i=1}^3 (k_{pi} \delta_{pix} \sin \varphi_i + k_{pi} \delta_{pix} \cos \varphi_i) = F_{bcy} - m_c g, \\ J_c \ddot{\theta}_c + c_{ct} r_{bc}^2 \dot{\theta}_c - \sum_{i=1}^3 c_{piy} r_{bc} \dot{\delta}_{piy} + k_{ct} r_{bc}^2 \theta_c - \sum_{i=1}^3 k_{piy} r_{bc} \delta_{piy} = -T_d. \end{aligned} \quad (10)$$

The vibration differential equation of the ring gear:

$$\begin{aligned} m_r \ddot{x}_r + c_r \dot{x}_r - \sum_{i=1}^3 c_{pir} \dot{\delta}_{pir} \sin(\varphi_i + \alpha) + k_r x_r - \sum_{i=1}^3 k_{pir} \delta_{pir} \sin(\varphi_i + \alpha) = 0, \\ m_r \ddot{y}_r + c_r \dot{y}_r + \sum_{i=1}^3 c_{pir} \dot{\delta}_{pir} \cos(\varphi_i + \alpha) + k_r y_r + \sum_{i=1}^3 k_{pir} \delta_{pir} \cos(\varphi_i + \alpha) = -m_r g, \\ J_r \ddot{\theta}_r + c_{rt} r_{br}^2 \dot{\theta}_r - \sum_{i=1}^3 c_{pir} r_{br} \dot{\delta}_{pir} + k_{rt} r_{br}^2 \theta_r - \sum_{i=1}^3 k_{pir} r_{br} \delta_{pir} = 0. \end{aligned} \quad (11)$$

The vibration differential equation of the i th planet gear:

$$\begin{aligned} m_{pi}(\ddot{x}_{pi} - 2\omega_c \dot{y}_{pi} - \omega_c^2 x_{pi}) + c_{pi} \dot{\delta}_{pix} + (c_{pis} \dot{\delta}_{pis} - c_{pir} \dot{\delta}_{pir}) \sin \alpha + k_{pi} \delta_{pix} \\ + (k_{pis} \delta_{pis} - k_{pir} \delta_{pir}) \sin \alpha = 0, \\ m_s(\ddot{y}_{pi} + 2\omega_c \dot{x}_{pi} - \omega_c^2 y_{pi}) + c_{pi} \dot{\delta}_{piy} + (c_{pis} \dot{\delta}_{pis} + c_{pir} \dot{\delta}_{pir}) \cos \alpha + k_{pi} \delta_{piy} \\ + (k_{pis} \delta_{pis} + k_{pir} \delta_{pir}) \cos \alpha = -m_s g, \\ J_{pi} \ddot{\theta}_{pi} - c_{pis} r_{bpi} \dot{\delta}_{pis} + c_{pir} r_{bpi} \dot{\delta}_{pir} - k_{pis} r_{bpi} \delta_{pis} + k_{pir} r_{bpi} \delta_{pir} = 0. \end{aligned} \quad (12)$$

The vibration differential equation of the sun gear:

$$\begin{aligned}
 m_s \ddot{x}_s - \sum_{i=1}^3 c_{pis} \dot{\delta}_{pis} \sin(\varphi_i - \alpha) - \sum_{i=1}^3 k_{pis} \delta_{pis} \sin(\varphi_i - \alpha) &= F_{bsx}, \\
 m_s \ddot{y}_s + \sum_{i=1}^3 c_{pis} \dot{\delta}_{pis} \cos(\varphi_i - \alpha) + \sum_{i=1}^3 k_{pis} \delta_{pis} \cos(\varphi_i - \alpha) &= F_{bsy} - m_s g, \\
 J_s \ddot{\theta}_s + c_{st} r_{bs}^2 \dot{\theta}_s - \sum_{i=1}^3 c_{pis} r_{bs} \dot{\delta}_{pis} + k_{st} r_{bs}^2 \theta_s - \sum_{i=1}^3 k_{pis} r_{bs} \delta_{pis} &= 0.
 \end{aligned} \tag{13}$$

The vibration differential equation of the intermediate-speed driving gear:

$$\begin{aligned}
 m_1 \ddot{x}_1 + c_{x1} \dot{x}_1 + k_{x1} x_1 &= -F_{x1} + m_1 \rho_1 \ddot{\theta}_1 \sin \varphi_1 + m_1 \rho_1 (\omega_1 + \dot{\theta}_1)^2 \cos \varphi_1, \\
 m_1 \ddot{y}_1 + c_{y1} \dot{y}_1 + k_{y1} y_1 &= -F_{y1} - m_1 g - m_1 \rho_1 \ddot{\theta}_1 \cos \varphi_1 + m_1 \rho_1 (\omega_1 + \dot{\theta}_1)^2 \sin \varphi_1, \\
 m_1 \ddot{z}_1 + c_{z1} \dot{z}_1 + k_{z1} z_1 &= -F_{z1}, \\
 (J_1 + m_1 \rho_1^2) \ddot{\theta}_1 + c_{t1} \dot{\theta}_1 + k_{t1} \theta_1 &= m_1 \rho_1 \ddot{x}_1 \sin \varphi_1 - m_1 \rho_1 \ddot{y}_1 \cos \varphi_1 - F_1 r_{b1}.
 \end{aligned} \tag{14}$$

The vibration differential equation of the intermediate-speed driven gear:

$$\begin{aligned}
 m_2 \ddot{x}_2 + c_{x2} \dot{x}_2 + k_{x2} x_2 &= F_{x2} + m_2 \rho_2 \ddot{\theta}_2 \sin \varphi_2 + m_2 \rho_2 (\omega_2 + \dot{\theta}_2)^2 \cos \varphi_2, \\
 m_2 \ddot{y}_2 + c_{y2} \dot{y}_2 + k_{y2} y_2 &= F_{y2} - m_2 g - m_2 \rho_2 \ddot{\theta}_2 \cos \varphi_2 + m_2 \rho_2 (\omega_2 + \dot{\theta}_2)^2 \sin \varphi_2, \\
 m_2 \ddot{z}_2 + c_{z2} \dot{z}_2 + k_{z2} z_2 &= F_{z2}, \\
 (J_2 + m_2 \rho_2^2) \ddot{\theta}_2 + c_{t2} \dot{\theta}_2 + k_{t2} \theta_2 &= m_2 \rho_2 \ddot{x}_2 \sin \varphi_2 - m_2 \rho_2 \ddot{y}_2 \cos \varphi_2 - F_2 r_{b2}.
 \end{aligned} \tag{15}$$

The vibration differential equation of the high-speed driving gear:

$$\begin{aligned}
 m_3 \ddot{x}_3 + c_{x3} \dot{x}_3 + k_{x3} x_3 &= -F_{x3} + m_3 \rho_3 \ddot{\theta}_3 \sin \varphi_3 + m_3 \rho_3 (\omega_3 + \dot{\theta}_3)^2 \cos \varphi_3, \\
 m_3 \ddot{y}_3 + c_{y3} \dot{y}_3 + k_{y3} y_3 &= -F_{y3} - m_3 g - m_3 \rho_3 \ddot{\theta}_3 \cos \varphi_3 + m_3 \rho_3 (\omega_3 + \dot{\theta}_3)^2 \sin \varphi_3, \\
 m_3 \ddot{z}_3 + c_{z3} \dot{z}_3 + k_{z3} z_3 &= -F_{z3}, \\
 (J_3 + m_3 \rho_3^2) \ddot{\theta}_3 + c_{t3} \dot{\theta}_3 + k_{t3} \theta_3 &= m_3 \rho_3 \ddot{x}_3 \sin \varphi_3 - m_3 \rho_3 \ddot{y}_3 \cos \varphi_3 - F_3 r_{b3}.
 \end{aligned} \tag{16}$$

The vibration differential equation of the high-speed driven gear:

$$\begin{aligned}
 m_4 \ddot{x}_4 + c_{x4} \dot{x}_4 + k_{x4} x_4 &= F_{x4} + m_4 \rho_4 \ddot{\theta}_4 \sin \varphi_4 + m_4 \rho_4 (\omega_4 + \dot{\theta}_4)^2 \cos \varphi_4, \\
 m_4 \ddot{y}_4 + c_{y4} \dot{y}_4 + k_{y4} y_4 &= F_{y4} - m_4 g - m_4 \rho_4 \ddot{\theta}_4 \cos \varphi_4 + m_4 \rho_4 (\omega_4 + \dot{\theta}_4)^2 \sin \varphi_4, \\
 m_4 \ddot{z}_4 + c_{z4} \dot{z}_4 + k_{z4} z_4 &= F_{z4}, \\
 (J_4 + m_4 \rho_4^2) \ddot{\theta}_4 + c_{t4} \dot{\theta}_4 + k_{t4} \theta_4 &= T_l + m_4 \rho_4 \ddot{x}_4 \sin \varphi_4 - m_4 \rho_4 \ddot{y}_4 \cos \varphi_4 - F_4 r_{b4}.
 \end{aligned} \tag{17}$$

3. Dynamic excitation of wind turbine gearbox

The gearbox transmission system withstands internal and external excitations. The external excitation mainly refers to the external influence factors, which cause the gearbox vibration. For example, the rotating blade vibration causes the gearbox vibration. The internal excitation mainly refers to gear meshing stiffness, meshing error and so on.

3.1. External excitation

According to the aerodynamic theory [21-22], taking the AR wind speed model as an external excitation, the excitation can be expressed as follows:

$$p_{in} = \frac{1}{2} \rho \pi R^3 v(t)^2 C_p, \tag{18}$$

where P_{in} is the input power of the wind turbine, ρ represents the air density, R indicates the radius of the wind turbine, $v(t)$ is the stochastic wind speed, C_p is power coefficient.

The input torque and output torque of the wind turbine can be expressed by the following equations:

$$T_{in} = \frac{P_{in}}{\omega}, \quad T_{out} = \frac{T_{in}}{i}, \quad (19)$$

where ω is the angular velocity of the wind turbine, i represents the transmission ratio of the gearbox.

According to the foregoing formulas, the simulation results of the wind speed and the wind turbine input torque are shown in Fig. 6.

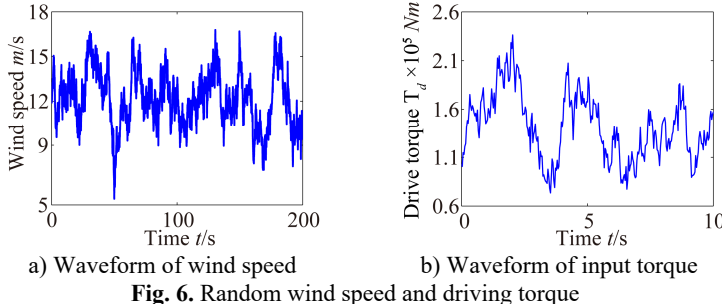


Fig. 6. Random wind speed and driving torque

3.2. Internal excitation

3.2.1. Dynamic model of the angular contact rolling bearing

Angular contact ball bearing model is shown in Fig. 7. Bearing outer ring is fixed in bearing chock, and inner ring is fixed in shaft. The balls are uniformly distributed between outer ring and inner ring. The velocities v_i and v_0 at the contact point between the rolling ball and outer/inner ring was analyzed, which can be expressed as:

$$v_i = \omega_i r, \quad v_0 = \omega_0 R, \quad (20)$$

where R and r represent the radius of the bearing outer and inner rings; ω_i and ω_0 are the angular velocities.

Assuming that it is the pure rolling between ball and outer/inner ring, and the velocity of cage can be expressed:

$$v_b = \frac{(v_o + v_i)}{2} = \frac{(\omega_0 R + \omega_i r)}{2}. \quad (21)$$

Generally, the bearing inner ring rotates together with shaft, and the bearing outer ring is fixed. Utilizing the relationships $\omega_0 = 0$, $\omega_i = \omega$. So the angular velocity of the cage is as follows:

$$\omega_b = \frac{2v_b}{(R + r)} = \frac{\omega_i r}{(R + r)}. \quad (22)$$

The rotation angle φ_i of the i th rolling ball at t moment can be expressed:

$$\varphi_i = \omega_b t + \frac{2\pi(i - 1)}{N_b}, \quad (i = 1, 2, 3, \dots, N_b), \quad (23)$$

where N_b represents the number of rolling ball.

In Fig. 7, d_b is the diameter of rolling ball, d indicates the diameter of shaft, d_i and d_o represent the diameters of the bearing outer and inner orbits, d_m is the diameter of pitch circle, and $d_m = (d_i + d_o)/2$.

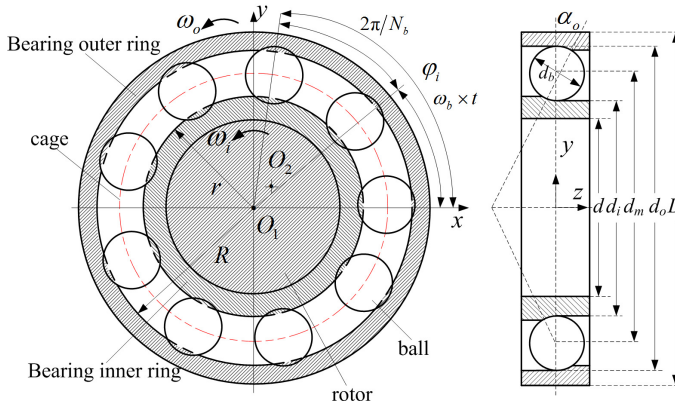
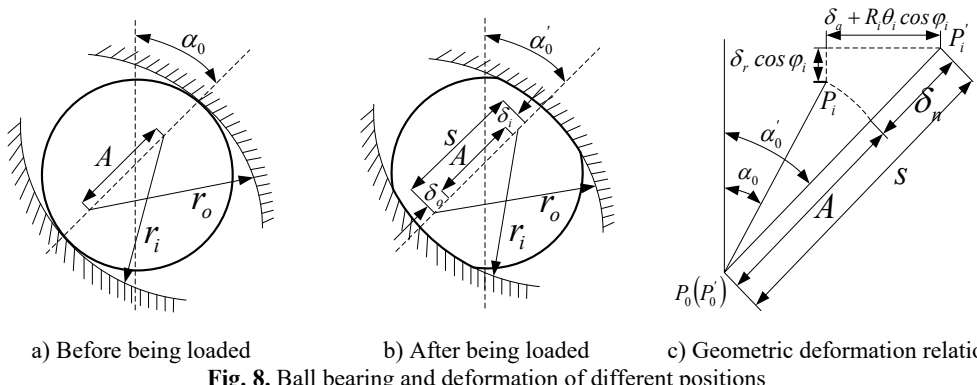


Fig. 7. Schematic diagram of angular contact rolling bearing

When the angular contact ball bearing is at a low speed, the centrifugal force and gyroscopic moment can be neglected. F_r and F_a represent the radial force and axial force of bearing respectively. The ball bearing and geometric deformation of different position are shown in Fig. 8. α_0 is the initial contacting angular of before being loaded, α'_0 indicates the angular after being loaded; P_0 represents the center of the bearing outer ring before being loaded; P'_0 is the one after being loaded. Because the outer ring is fixed, the P_0 and P'_0 are the same position; P_i is the center of inner ring before being loaded; P'_i represents the after being loaded; δ_{ai} , δ_{ri} and θ_i are the axial deformation, radial deformation and angular deformation respectively; R_i is the curvature radius of inner orbit; φ_i is the position angular; δ_i , δ_0 and δ_{bi} represent the contacting deformation and total deformation between rolling ball and outer and inner orbits.



a) Before being loaded

b) After being loaded

c) Geometric deformation relation
Fig. 8. Ball bearing and deformation of different positions

Because the centrifugal force and gyroscopic moment are ignored, the contacting angular between rolling ball and bearing orbit and the contacting force are the same. In Fig. 8(b), the deformation of rolling ball at position angular φ_i can be expressed as:

$$\delta_{bi} = \delta_i + \delta_0 = S - A. \quad (24)$$

According to geometric relationship in Fig. 8(c), the distance S between the curvature center

of inner orbit and outer orbit can be expressed by the following equation:

$$S = [(A\sin\alpha_o + z + R_i\theta_i \cos\varphi_i)^2 + (A\cos\alpha_o + x\cos\varphi_i + y\sin\varphi_i)^2]^{1/2}. \quad (25)$$

The normal contacting deformation between the i th rolling ball and the bearing orbit is as follow:

$$\delta_{bi} = S - A = [(A\sin\alpha_o + \delta_a + R_i\theta_i \cos\varphi_i)^2 + (A\cos\alpha_o + \delta_r)^2]^{1/2} - A. \quad (26)$$

Utilizing the relationships $\delta_a = z$, $\delta_r = x\cos\varphi_i + y\sin\varphi_i$, the Eq. (26) can be expressed by:

$$\delta_{bi} = S - A = [(A\sin\alpha_o + z + R_i\theta_i \cos\varphi_i)^2 + (A\cos\alpha_o + x\cos\varphi_i + y\sin\varphi_i)^2]^{1/2} - A, \quad (27)$$

where x , y and z represent the linear vibration displacement respectively; $R_i = d_m/2 + (r_i - (d_b/2))\cos\alpha_0$; A is the initial distance between curvature center of inner orbit and outer orbit, and $A = r_i + r_0 + \gamma_0 - d_b$.

At the positon angular φ_i , the actually contacting angular α'_0 can be expressed as:

$$\tan\alpha'_0 = \frac{A\sin\alpha_o + z + R_i\theta_i \cos\varphi_i}{A\cos\alpha_o + x\cos\varphi_i + y\sin\varphi_i}. \quad (28)$$

According to nonlinear Hertz contact theory, the contact force between the i th rolling ball and the bearing orbits is f_{bi} , at the same time, the normal stress can be only generated between the rolling ball and the bearing orbits when the δ_{bi} is more than zero. So the force can be expressed by:

$$\begin{aligned} f_{bi} &= K_c(\delta_{bi})^{3/2} \cdot H(\delta_{bi}) \\ &= K_c \left\{ [(A\sin\alpha_o + z + R_i\theta_i \cos\varphi_i)^2 + (A\cos\alpha_o + x\cos\varphi_i + y\sin\varphi_i)^2]^{1/2} - A \right\}^{3/2} \\ &\quad \cdot H \left\{ [(A\sin\alpha_o + z + R_i\theta_i \cos\varphi_i)^2 + (A\cos\alpha_o + x\cos\varphi_i + y\sin\varphi_i)^2]^{1/2} - A \right\}. \end{aligned} \quad (29)$$

The normal load can be known by the Eq. (29), and the axial and radial forces can be expressed as below:

$$f_{ri} = f_{bi}\cos\alpha'_0 = K_c(\delta_{bi})^{3/2}\cos\alpha'_0, \quad f_{ai} = f_{bi}\sin\alpha'_0 = K_c(\delta_{bi})^{3/2}\sin\alpha'_0. \quad (30)$$

So the bearing forces (F_{bx} , F_{by} and F_{bz}) in x , y and z directions can be expressed by:

$$\begin{aligned} F_{bx} &= \sum_{i=1}^{N_b} f_{ri} \cos\varphi_i = \sum_{i=1}^{N_b} K_c(\delta_{bi})^{3/2} \cos\alpha'_0 H(\delta_{bi}) \cos\varphi_i, \\ F_{by} &= \sum_{i=1}^{N_b} f_{ri} \sin\varphi_i = \sum_{i=1}^{N_b} K_c(\delta_{bi})^{3/2} \cos\alpha'_0 H(\delta_{bi}) \sin\varphi_i, \\ F_{bz} &= \sum_{i=1}^{N_b} f_{ai} = \sum_{i=1}^{N_b} K_c(\delta_{bi})^{3/2} \sin\alpha'_0 H(\delta_{bi}). \end{aligned} \quad (31)$$

3.2.2. Error excitation

Using the harmonic function [23], the error excitation can be described as follows:

$$e(t) = e_0 + e_r \sin(\omega_e t + \phi_e), \quad (32)$$

where e_0 and e_r represent the mean and amplitude of meshing error; φ_e is initial position angle. $\omega_e = 2\pi n_1 z_1 / 60$. z_1 indicates the tooth number of driving gear.

4. Nonlinear dynamic response of gearbox system

From the previous conclusions and results, it can be seen that the wind turbine gearbox is a complicated system with the strong nonlinearity, multi-speed gear-driven, time variance and the support bearing. Therefore it is necessary to give a detailed analysis of the wind turbine gearbox. The dynamic behaviors of system are investigated by Runge-Kutta numerical simulation method. On this basis, the gearbox geometry parameters of the transmission system analyzed in this paper are given in Table 1.

Table 1. Geometric parameters of the wind gearbox transmission system

	Ring gear	Sun gear	Planet gear	Modulus	Pressure angle
Low-speed planetary gear stage	123	27	48	12	22.5
Medium-speed helical gear stage	Driving gear 1	Driven gear 2	Normal modules	Helix angle	Pressure angle
	104	23	10	13.5	22.5
High-speed helical gear stage	Driving gear 3	Driven gear 4	Normal modules	Helix angle	Pressure angle
	98	25	6.5	15	20

4.1. Dynamic response of the wind turbine gearbox

By applying the coupled vibration model of a wind turbine gearbox transmission system, the vibration analysis and calculations are carried out. In this paper, the dynamic response of the MW wind turbine gearbox with the external load excitation, meshing stiffness, input and output torques, meshing error, nonlinear characteristics of the support bearing and gravity effects are investigated using the Runge-Kutta numerical simulation method that includes simultaneous internal and external excitations. This method using the elastic mechanics theory is applied to a lumped-parameter wind turbine gearbox model. The coupled dynamic mechanical analysis of the system is performed so as to include all the components of influence factors.

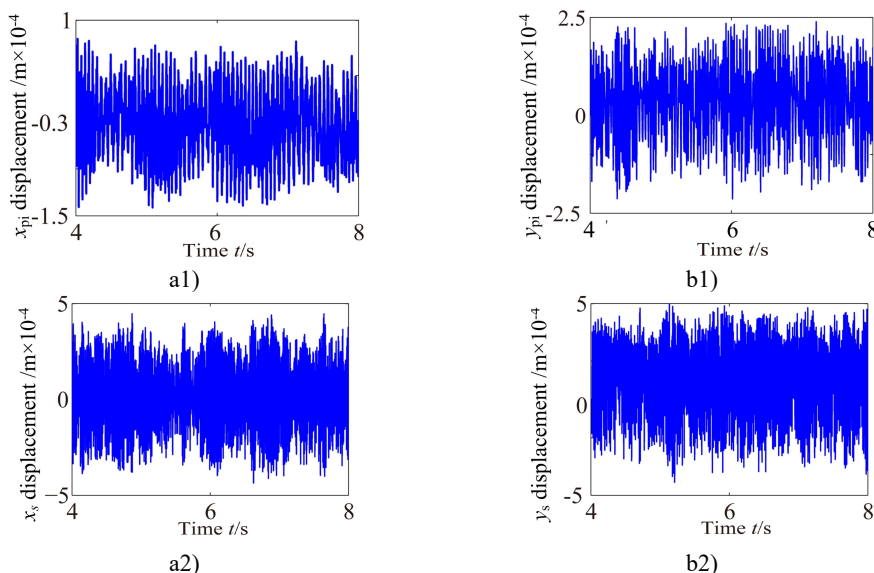


Fig. 9. Vibration waveform of the planet and sun

Fig. 9-Fig. 11 and Fig. 12-Fig. 14 show the vibration response of the partial component in x ,

y , θ directions, in which the carrier driver, having a rated speed of 17 r.p.m., drives the wind turbine gearbox to rotate. The response curves (vibration waveform and spectrum) of components are made appropriate interception in order to analyze the dynamic characteristics of the wind turbine gearbox train system more accurately. The lateral vibration displacement response of planet gear and sun gear in the low-speed stage is shown in Fig. 9. The negative value in figure indicates the opposite direction with respect to the predetermined positive direction in the model. In this paper, it can be found from comparison with Fig. 9-Fig. 11 that the planet gear has the minimum vibration amplitude, the vibration amplitude of medium-speed helical gear stage takes second place, and the vibration amplitude of high-speed helical gear stage has the maximum. In addition, the vibration waveform of each component in the train system presents a different changing trend due to the influences of the internal and external excitations.

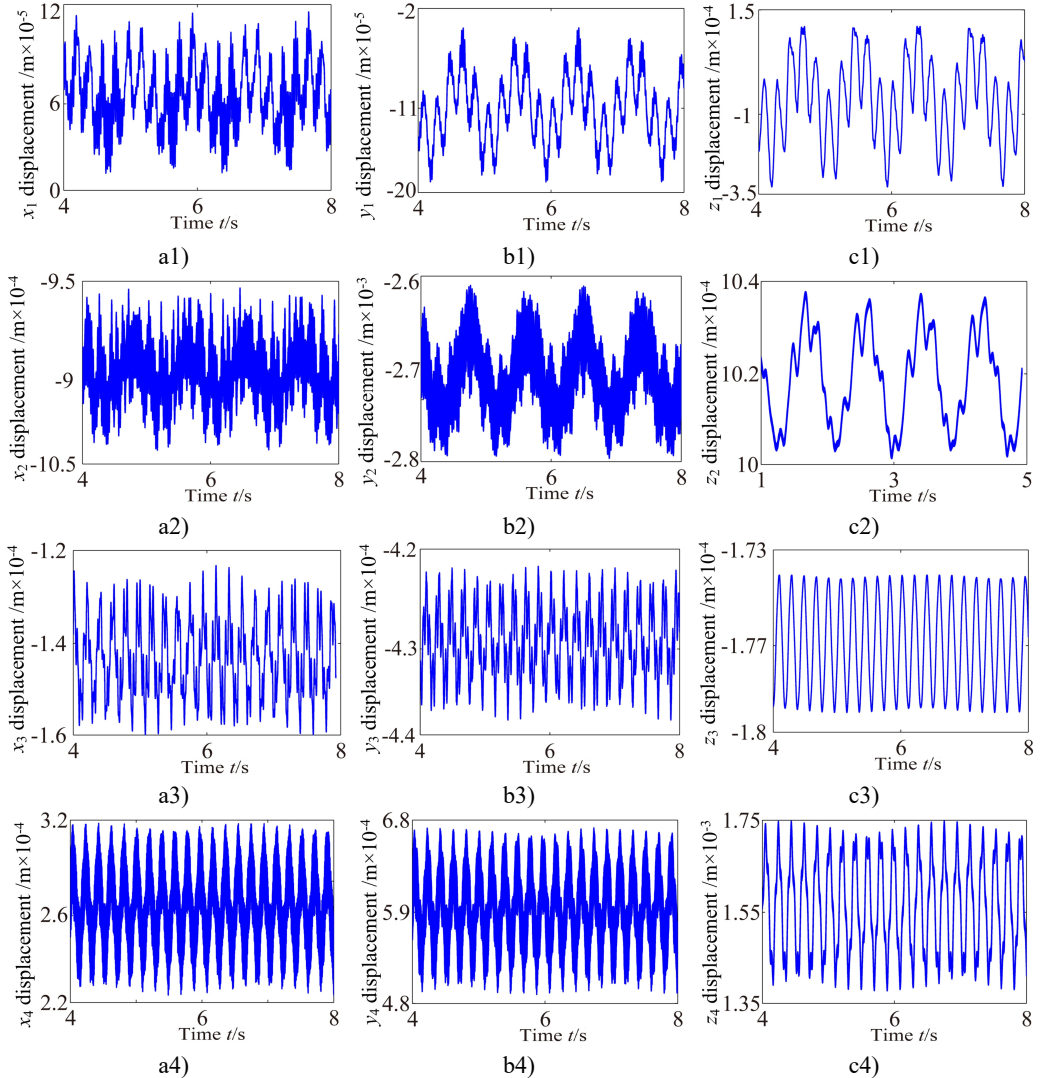


Fig. 10. Vibration waveform of the gear in medium-speed stage and high-speed stage

It can be seen from Fig. 9 that the dynamic characteristics of the planet gear and sun gear in low-speed stage become more complex due to the time-varying load and nonlinear characteristics of the support bearing. The vibration responses of the planet and sun are significant higher than

others in low-speed planetary gear stage. (Because of the limited space, this paper only gives the vibration response of planet and sun). Moreover, high-harmonic components are significant shown in time-domain response. It can be found from comparison Fig. 9 with Fig. 6 that the vibration responses of the planet and sun are similar change with the external excitation.

Fig. 10 shows the lateral and axial vibration displacement responses of the medium-speed helical gear stage and high-speed helical gear stage. It can be seen from Fig. 10 that the vibration responses of driving gear in x , y , z directions are slight higher than one of the driven gear. Comparing Fig. 10 with Fig. 9, it can be seen that the vibration response of the medium-speed helical gear stage become more complex due to the effects on the low-speed planetary gear stage and high-speed helical gear. In addition, it can be also found the low-speed stage is mainly affected by the external load, and the vibration of the high-speed stage mainly causes by load. The vibration amplitudes are also obviously increasing and the magnitude of amplitude reach the 0.1 mm due to the effects of the internal and external excitation. The support bearings in the low-speed stage and high-speed stage inevitably stand heavy dynamic load due to the effect of the gear eccentricity, mesh error and gravity. Hence, the bearing appears earlier failure. The dynamic response analysis for the wind turbine gearbox should fully be considered the influences of the bending vibration, torsional vibration, axial vibration and coupled vibration.

Fig. 11 shows angular vibration displacement response of the partial component. This comparison proves that the torsional vibration displacement of each component is obviously higher than those of lateral and axial vibration displacement response. So the torsional vibration is the main vibration and torsional amplitude obviously appears different vibration features due to the effects of the external excitation. In addition, the torsional vibration responses of the components appear complex vibration characteristics, which are caused by the nonlinear features of the support bearing and other excitations. In fact, bearing is one of main factor controlling vibration in a power transmission system because they play a key role in determining the system's natural frequencies, and they can also be responsible for vibration amplification and transmission to other parts.

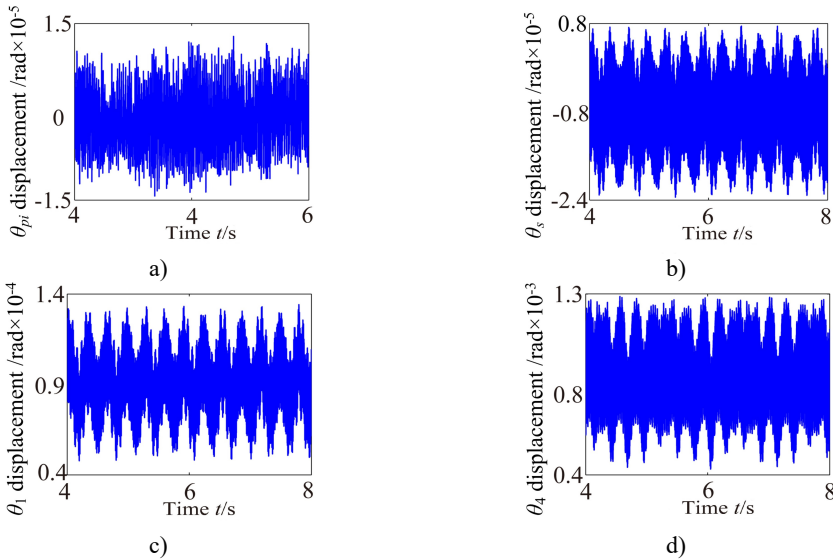


Fig. 11. Torsional vibration of the partial component in gearbox

4.2. Frequency response of the gearbox

In order to accurately analyze the dynamic of the wind turbine gearbox transmission system, Figs. 12-14 show the frequency domain response of the partial component in lateral-direction,

axial-direction and torsional-direction. It can be seen that the frequency domain response appear a lot of frequency multiplication and frequency combination components. The meshing frequency component of the low-speed stage is f_m ($f_m = f_c z_r = 29.45$ Hz), medium-meshing frequency component is f_{m1} ($f_{m1} = z_1 n_1 / 60 = 163.6$ Hz), and the meshing frequency component of the high-speed stage f_{m2} ($f_{m2} = z_3 n_3 / 60 = 707$ Hz) in the wind turbine gearbox transmission system. Fig. 12 show the lateral frequency domain response of planet gear and sun gear in the low-speed stage. Analysis of the Fig. 12(a), (b) shows that there is a certain degree of continuous spectrum at low-frequency stage due to the effects of the support bearing and the meshing between the gears, which mainly includes frequency combination ($2f_m + f_{bc}$, $4f_m + f_{bp}$, $5f_m + 3f_{bp} + f_{bc}, \dots$) and frequency multiplication. Besides, it also appears a high-harmonic component 536.5 Hz ($18f_m + 3f_s + f_p$). For the sun gear spectrum Fig. 12(c), (d), the frequency components are relatively simple, but it also appears complex frequency combination ($2f_m + f_s$, $4f_m + 10f_p$, $5f_m + 3f_{bs} - f_s, \dots$) and frequency multiplication. In addition to the high-harmonic component 536.5 Hz, there is also another obvious high-harmonic component 571.5 Hz ($19f_m + f_{bs}$). The result indicate that the vibration frequency low-speed stage has a very obvious probability distribution, which is mainly concentrated in the frequency range below 200 Hz. This phenomenon is caused by the nonlinear characteristics of the support bearing and external excitation.

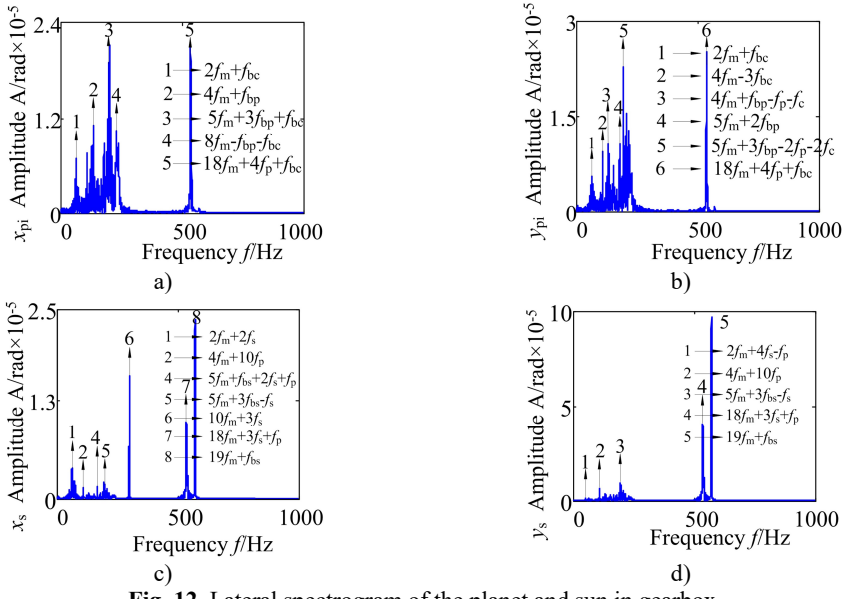


Fig. 12. Lateral spectrogram of the planet and sun in gearbox

Fig. 13 shows the lateral and axial frequency domain response of the medium-speed helical gear stage and high-speed helical gear stage. It can be seen from Fig. 13 that the own rotating frequency and the rotating frequency with meshing gear are the main frequencies in x , y , z directions. For example, the driving rotating frequency f_1 ($f_1 = n_1 / 60 = 1.57$ Hz) and the driven rotating frequency f_2 ($f_2 = n_2 / 60 = 7.13$ Hz) in medium-speed helical gear stage. The driving rotating frequency f_3 ($f_3 = n_3 / 60 = 7.13$ Hz) and the driven rotating frequency f_4 ($f_4 = n_4 / 60 = 28.71$ Hz) in high-speed helical gear stage. The meshing frequencies f_{m1} ($f_{m1} = z_1 n_1 / 60 = 163.6$ Hz) and ($f_{m2} = z_3 n_3 / 60 = 707$ Hz) are not immediately obvious, which aren't mark in the spectrogram.

It can be seen from the medium-speed helical gear stage that the driving shaft rotating frequency f_1 is the main frequency component in x -direction and y -direction, and the driven shaft

rotating frequency f_2 is the main frequency component in y -direction. The bearing variable stiffness frequencies f_{b1} (17.17 Hz) and f_{b2} (58.59 Hz) also appear in three directions. In addition, the frequency combination ($f_2 - f_1$, $f_2 + f_1$, $f_{b1} + f_1$, $f_{b2} + f_1$, ...) and frequency multiplication ($2f_1$, $2f_2$, $2f_{b1}$, $2f_{b2}$, ...) make the spectrogram become more complex in x and y directions. What's more, the frequency components are relatively simple in z direction. The rotating frequency and frequency combination are the main components and the bearing variable stiffness frequencies do not obviously appear. So the bearing has a larger effect on the lateral vibration. (High-speed train stage also has the same properties, be limited by the space restrict can't write all go into detail).

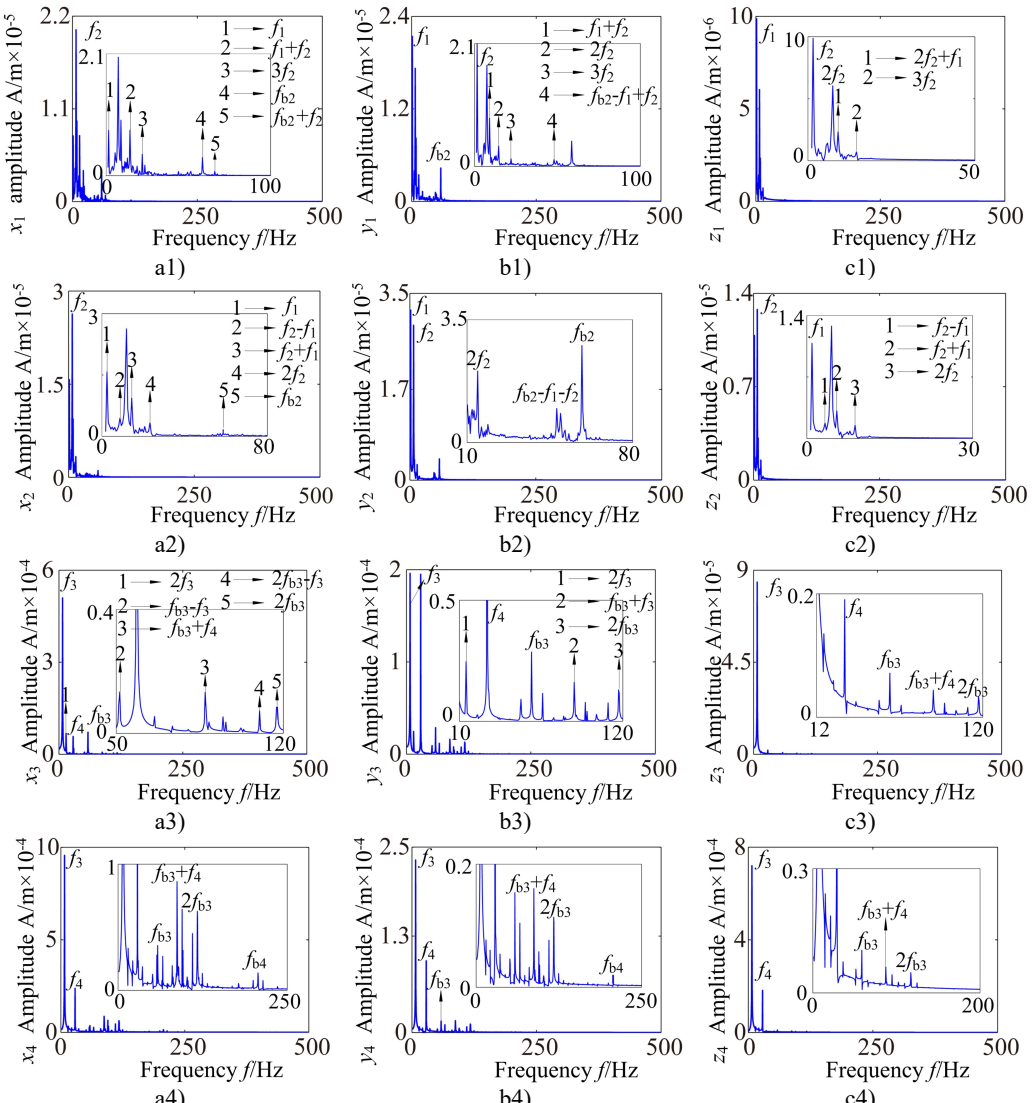


Fig. 13. Lateral and axial spectrogram of medium-speed stage and high-speed stage in gearbox

Fig. 14 shows torsional frequency domain response of the partial component in gearbox. Through the contrastive analysis, it may discover that with the increase of the speed, the amplitude distribution becomes complex gradually, where the frequency combination and frequency multiplication also appear (it is similar with the forgoing waveform). The further analysis shows

that these phenomena are caused by the influences of the external excitation, the characteristics of assembly, the gear geometry parameters and the non-linear characteristics of the support bearing.

5. Conclusion

The drive-train in this study is consisted of a low-speed planetary gear stage and two high-speed helical gear stages. Based on the theory of elasticity mechanics, a lumped-parameter mathematical model is used to more precisely analyze the nonlinear dynamic model of coupled vibration for the wind turbine gearbox transmission system. The main conclusions are as follows:

1) The dynamic response of each component in the gearbox transmission system is mainly superposed by high-frequency component caused by the internal excitation and low-frequency component caused by the external excitation. The vibration frequency of the wind power planetary gear transmission system has a very obvious probability distribution, which is mainly concentrated in the frequency range below 200 Hz.

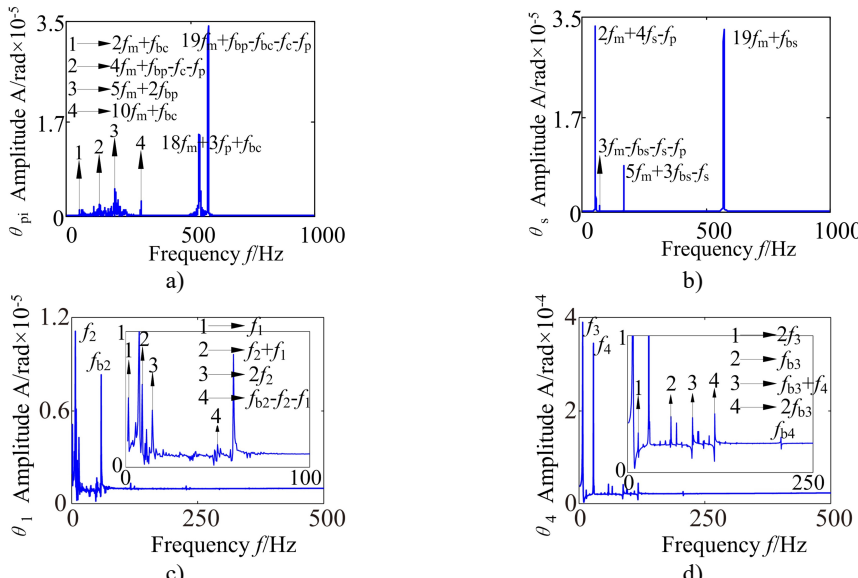


Fig. 14. Torsional spectrogram of the partial component in gearbox

2) This comparison proves that the angular vibration displacement of each component is obviously higher than those of lateral and axial vibration displacement response. So the torsional vibration is the main vibration, which is similar change with the external excitation. The planet gear has the minimum vibration amplitude, the vibration amplitude of medium-speed helical gear stage takes second place, and the vibration amplitude of high-speed helical gear stage has the maximum.

3) In medium-level and high-level transmissions, an obvious component of rotational frequency of driven shaft exists in the driving shaft due to the coupled lateral-torsional-axial vibration, and the rotating frequency and the frequency combination components are more obvious showed in torsional direction. Bearing is one of main factor controlling vibration in a power transmission system because they play a key role in determining the system's natural frequencies, and they can also be responsible for vibration amplification and transmission to other parts. In addition, the bearing has its own variable stiffness frequency, which should be avoided in engineering system design stage.

Acknowledgements

The project was supported by China Natural Science Funds (No. 51475084).

References

- [1] Peeters J. L. M., Vandepitte D., Sas P. Analysis of internal drive train dynamics in a wind turbine. *Wind Energy*, Vol. 9, 2006, p. 141-161.
- [2] Peeters J. L. M. *Simulation of Dynamic Drive Train Loads in a Wind Turbine*. Katholieke Universiteit Leuven, Belgium, 2006.
- [3] Guo Y., Keller J., Parker R. Dynamic analysis of wind turbine planetary gears using an extended harmonic balance approach. *ASME Conference Proceedings*, Leuven, Belgium, 2012.
- [4] Riziotis V. A., Voutsinas S. G. Fatigue loads on wind turbines of different control startegies operating in complex terrain. *Journal of Wind Engineering and Industrial Aerodynamics*, Vol. 85, 2000, p. 211-240.
- [5] Thomsen K., Pouls S. Fatigue loads for wind turbines operating in wakes. *Journal of Wind Engineering*, Vol. 80, 1999, p. 121-136.
- [6] Peeters J., Vandepitte D., Sas P. Flexible multibody model of a three-stage planetary gear-box in a wind turbine. *Proceedings of ISMA*, Vol. 165, 2004, p. 3923-3942.
- [7] Yang W. X., Court R., Jiang J. S. Wind turbine condition monitoring by the approach of SCADA data analysis. *Renewable Energy*, Vol. 53, 2013, p. 365-376.
- [8] Pérez J. M. P., Márquez F. P. G., Tobias A. Wind turbine reliability analysis. *Renewable and Sustainable Energy Reviews*, Vol. 23, 2013, p. 463-472.
- [9] Tavner P. J., Xiang J., Spinato F. Reliability analysis for wind turbines. *Wind Energy*, Vol. 10, Issue 1, 2007, p. 1-18.
- [10] Zhou Z. G., Qin D. T., Yang J., et al. Gear-bearing coupling dynamics characteristics of wind turbine planetary gear transmission system under variable load. *Journal of Chongqing University*, Vol. 35, 2012, p. 7-14.
- [11] Zhu C. H., Huang Z. H., Tang Q., et al. Analysis of nonlinear coupling dynamic characteristics of gearbox system about wind-driven generation. *Chinese Journal of Mechanical Engineering*, Vol. 41, 2005, p. 203-207.
- [12] Bartelmus W., Zimroz R. Vibration condition monitoring of planetary gearbox under varying external load. *Mechanical Systems and Signal Processing*, Vol. 23, 2009, p. 246-257.
- [13] Qin D. T., Gu X. G., Wang J. H. Dynamic analysis and optimization of gear trains in a megawatt level wind turbine. *Journal of Chongqing University*, Vol. 32, 2009, p. 408-414.
- [14] Qin D. T., Wang J. H., Lim T. C. Flexible multibody dynamic modeling of a horizontal and turbine drive train system. *Journal of Sound and Vibration*, Vol. 329, 2010, p. 3565-3586.
- [15] Xu Q., Chen C. Z. The model for dynamic of wind turbine gear transmission system. *Journal of Vibration and Shock*, Vol. 29, 2009, p. 7-12.
- [16] Helsen J., Vanhollebeke F., Marrant B. Multi-body modeling of varying complexity for modal behavior analysis of wind turbine gearboxes. *Renewable Energy*, Vol. 36, 2011, p. 3098-3113.
- [17] Helsen J., Vanhollebeke F., Conincka F. D., et al. Insights in wind turbine drive train dynamics gathered by validating advanced models on a newly develop 13.2 MW dynamically controlled test-rig. *Mechatronics*, Vol. 21, 2011, p. 737-752.
- [18] John F. H., Christine A. M., et al. Wind energy conversion with a variable ratio gearbox design and analysis. *Renewable Energy*, Vol. 36, 2011, p. 1075-1080.
- [19] Shi W., Kim C. W., Chung C. W., Park H. C. Dynamic modeling and analysis of a wind turbine drive-train using the torsional dynamic model. *International Journal of Precision Engineering and Manufacturing*, Vol. 14, 2013, p. 153-159.
- [20] Dou W., Zhang N., Liu Z. S. The coupled bending and torsional vibrations of the high-speed geared rotor-bearing system. *Journal of Vibration Engineering*, Vol. 24, 2011, p. 385-393.
- [21] Lmi T. C., Cheng Y. A theoretical study of the effect of pinion offset on the dynamics of hypoid geared rotor system. *Transactions of the ASME, Journal of Mechanical Design*, Vol. 121, 1999, p. 535-539.
- [22] Liu C. Y., Wang W. S., Zhao H. X., et al. Induction Generators for Wind Power. *China Electric Power Publishing House*, Beijing, Vol. 8, 2009, p. 42-47.

- [23] Li R. F., Tao Z. G., Lin T. J., et al. Numerical simulation for inner dynamic excitation of gearing. Journal of Mechanical Transmission, Vol. 25, 2001, p. 1-3.



Zhaohui Ren is currently a Professor at the School of Mechanical Engineering and Automation, Northeastern University. He received his Ph.D. degree from Northeastern University in 2005. His research interests include rotor dynamics, fault diagnosis and product integrated design method.



Shihua Zhou is a Ph.D. student at the School of Mechanical Engineering and Automation, Northeastern University. He received his Master's degree from Northeastern University, China, in 2013. His research interest is the dynamic characteristics of gear-rotor-bearing system.



Bangchun Wen is a Professor at School of Mechanical Engineering and Automation, Northeastern University, China. He graduated as a postgraduate from Department of Mechanical Engineering at Northeast University of Technology in 1957. Professor Wen systematically studied and developed the new course of "Vibration Utilization Engineering" combined with vibration theory and machinery.